Iranian Journal of Astronomy and Astrophysics
Vol. 11, No. 4, Autumn 2024, 275–290
©Available online at http://ijaa.du.ac.ir
DOI: 10.22128/ijaa.2025.931.1203
Online ISSN: 2383–403X

Iranian Journal of Astronomy and Astrophysics

Research Paper

On the Generation and Dissipation of Magnetic Energy During a Shear-Flow Driven Instability in Space Plasmas

Mahboub Hosseinpour
Faculty of Physics, University of Tabriz, Tabriz, P.O.Box:16471, Iran;
E-mail: hosseinpour@tabrizu.ac.ir

Received: 26 December 2024; **Accepted:** 16 February 2025; **Published:** 19 February 2025

Abstract. A well-known shear flow-driven instability, namely the Kelvin-Helmholtz instability (KHI), establishes important changes in the macroscopic dynamics of some space magnetized plasmas such as the solar corona, astrophysical jets and the Earth's magnetopause. We use two-dimensional resistive magnetohydrodynamic (MHD) simulations to investigate the generation and dissipation of magnetic energy during KHI in a compressible plasma with an initial uniform magnetic field parallel to the direction of streaming flow. Regardless of the resistivity value, the results show that, up to a specific time, amplification of magnetic energy, in particular in the linear and early nonlinear phases of KHI happens by the flow's work on the magnetic field. This work is mainly efficient on the boundaries of growing vortices of KHI. As the KHI proceeds into the fully nonlinear (turbulent) phase, magnetic energy dissipation via Ohmic heating becomes significant, and eventually balances the flow's work, so the magnetic energy becomes saturated. We also found that increasing the plasma resistivity weakens the mechanism of generating magnetic energy, and may even be completely suppressed in a highly collisional fluid.

Keywords: Kelvin-Helmholtz instability, Shear-flow, MHD simulation, Space plasma, Plasma resistivity

1 Introduction

The relative motion of two plasma fluids separated by a thin interface layer can be unstable to the Kelvin–Helmholtz instability (KHI; [1–3]). Rolling up of the interface and subsequent vortex formation is a typical signature of the KHI. The KH dynamics then develop into a nonlinear stage involving large-size vortices, and eventually, the turbulent motions appear where vortices merge and monster vortices emerge. Strong gradients of plasma and magnetic pressures and magnetic tension force define KHI's primary and fundamental dynamics.

KHI is a well-known viable mechanism for momentum and energy exchange and transport between two different plasma fluids. It is important for the understanding of space and astrophysical phenomena involving a sheared plasma flow, such as the interaction between the solar wind and planetary magnetospheres and ionospheres [4–9] and the structure of cometary tails [10]. KHI has also been applied in MHD models of pulsar magnetospheres and extragalactic radio jets [11–14]. KHI has been extensively studied in the low solar

corona. For instance, ripples at the prominence surface [15], billows on the flank of coronal mass ejecta [16–18] and traveling fluctuations at the boundaries of magnetic structures [19] have been attributed to the KH instability.

Until now, KHI has been extensively studied analytically, numerically, experimentally, and observationally by taking into account different physics, effects, and various ranges of main parameters such as compressibility, viscosity, externally imposed magnetic field, mass density, and temperature ratio, etc. (e.g. [20] and references therein). Nevertheless, plasma resistivity is another main parameter determining the degree of plasma collisionality that has gotten less attention than other effects in studying the KHI. Although, one of the major characteristics of space and astrophysical plasmas is their low collisionality compared with laboratory plasmas, however, there are some respective astrophysical contexts with a dense plasma, where, quite often, the plasma is not fully ionized, so that the effect of collisions with the neutral particles should be taken into account. Therefore, plasma resistivity is thought to bring important changes to the dynamics of KHI and the associated MHD modes, especially when the plasma is highly magnetized. The non-ideal effect of resistivity is the main cause of magnetic energy dissipation via the well-known mechanism of Joule (Ohmic) heating or dissipation in magnetized plasmas. In plasmas, an external magnetic field parallel to the streaming flow stabilizes the KHI via the magnetic tension force [21]. Furthermore, resistive effects are thought also to suppress the growth and even the formation of the KHI [22]. Therefore, the essential role of plasma resistivity in the dynamics of KHI deserves more attention and study.

Some analytical works have been published regarding the resistivity effects, which investigated the corresponding effects only in the linear regime of KHI. For example, [23] have discussed analytically the KHI of two rotating fluids. One of the fluids is conducting with a finite resistivity, while the other is non-conducting, and the magnetic field is oblique to the fluid interface. Based on the obtained general dispersion relation, they concluded that a stable mode becomes overstable, and grows exponentially with the resistivity with scaling $\eta^{1/3}$. This conclusion, however, is in contradiction with our numerical results that generally the growth rate even in the linear regime decreases with increasing η (see Sec. 3). However, it should be mentioned that according to our simulation setup, both fluids are conductive with the same resistivity, while in the study of [23], the resistivity in one of the fluids is infinite (non-conducting fluid).

In another study, [24] studied numerically the magnetic reconnection process induced by the KHI in resistive plasmas. They changed the value of resistivity in the limited range as $\eta = 0.005, 0.01, 0.05$ and showed that the essential features of KHI hold almost the same regardless of the change in the resistivity. Note that, our results indicate a significant dependency of, at least, magnetic energy temporal evolution to the resistivity.

Furthermore, [25] investigated numerically the effects of resistivity and viscosity on the onset and growth of the Kelvin-Helmholtz instability (KHI) in an oscillating coronal loop. Based on MHD simulations, they concluded that increasing either viscosity or resistivity suppresses the KHI. In other words, larger resistivity values delay the formation of the instability and, in some cases, prevent the onset completely. This conclusion is consistent with our results presented below.

The most similar work to our study has been presented by [26]. They have reported 2D simulations exploring the nonlinear evolution of the Kelvin Helmholtz instability in both a magnetized and unmagnetized shear flow. We have extended the simulations to the very smaller values of the plasma resistivity and investigated the population of X-points and its dependency on the plasma resistivity. Furthermore, we have addressed in more detail the general features of a typical reconnection event occurring inside a current sheet and the growth of plasmoid instability.

In our current study, by varying the plasma resistivity over four orders of magnitude with the minimum dimensionless value of $\eta = 1.0 \times 10^{-7}$, we carry out two-dimensional resistive MHD simulations of KHI in a magnetized compressible plasma. Specifically, we investigate the effect of resistivity on the spatial and temporal evolution of magnetic energy and examine the mechanism of magnetic energy generation and Ohmic dissipation via the magnetic reconnection process. To do so, the rest of the paper is structured as follows: in the next section, the simulation setup and initial model are presented. The results are given in Sec. 3, followed by a summary and conclusion in Sec. 4.

2 Simulation Setup

Two-dimensional MHD simulations use the PLUTO code, a publicly available numerical code for astrophysical plasma simulations developed at the University of Turin [27]. PLUTO solves conservative partial differential MHD equations, equation (1) including the non-ideal effect of resistivity. It is an Eulerian, finite volume, shock-capturing code based on high-order Godunov methods providing several integration algorithms, Riemann solvers, time-stepping methods, and interpolation schemes. The set of single-fluid resistive MHD equations in the conservative form to be solved numerically is

$$\begin{aligned}
&\frac{\partial \rho}{\partial t} + \nabla.(\rho \mathbf{V}) = 0, \\
&\frac{\partial \mathbf{m}}{\partial t} + \nabla.[\mathbf{m}\mathbf{V} - \mathbf{B}\mathbf{B} + \mathbf{I}(P + \frac{\mathbf{B}^2}{2})] = 0, \\
&\frac{\partial \mathbf{B}}{\partial t} + \nabla \times \mathbf{E} = 0, \\
&\frac{\partial E_t}{\partial t} + \nabla.[(\frac{\rho \mathbf{V}^2}{2} + \rho e + P)\mathbf{V} + \mathbf{E} \times \mathbf{B}] = 0,
\end{aligned} \tag{1}$$

where the generalized Ohm's law defines the electric field, $\mathbf{E} = -\mathbf{V} \times \mathbf{B} + \eta.\mathbf{J}$ with η as the plasma resistivity tensor and the electric current density $\mathbf{J} = \nabla \times \mathbf{B}$. Here, the permeability constant is set to one, $\mu_0 = 1$. We assume a uniform and the same resistivity (η) on both sides of the interface, which is set to nine different values according to Table 1, that also lists the corresponding dimensionless Lundquist numbers defined as $S = L_x V_A/\eta$ with L_x and $V_A = B_0/\sqrt{\rho}$ being the simulation box size and the Alfvèn velocity defined below. The minimum and maximum values of resistivity in our study are $\eta = 1.0 \times 10^{-7}$ and $\eta = 5.0 \times 10^{-3}$, respectively. This means that the corresponding maximum value of the Lundquist number is $S = 1.5 \times 10^5$. We should admit that the in situ resistivity value in space plasmas, especially in the solar corona is far less than those achievable in numerical simulations. Furthermore, $E_t = \rho e + \frac{\mathbf{m}^2}{2\rho} + \frac{\mathbf{B}^2}{2}$ is the total energy density with e, ρ, $\mathbf{m}$ and $\mathbf{B}$ being the internal energy density, mass density, momentum density, $\mathbf{m} = \rho \mathbf{V}$, and magnetic field respectively. Finally, $\mathbf{V}$ and $\mathbf{I}$ are the bulk velocity of plasma and the unitary tensor. An ideal equation of state provides the closure for MHD equations in the form $\rho e = P/(\Gamma - 1)$, where P and Γ are thermal pressure and the constant ratio of specific heats. The divergence-zero constraint for the magnetic field, $\nabla.\mathbf{B} = 0.$, is being checked by the code at every time-step of integration of equations.

To set up the conditions for the growth of Kelvin-Helmholtz instability, the mass density is given as $\rho(y) = (\rho_1 + \rho_2)/2 + ((\rho_2 - \rho_1)/2)\ \tanh(y/\Delta)$ with a narrow half width $\Delta = 0.01$, $\rho_1 = 1.0$ and $\rho_2 = 0.5$. Meanwhile, as an essential condition, the plasma velocity hyperbolic tangent profile is defined by $\mathbf{V}(y) = V_0\ \tanh(y/\Delta)\hat{x}$ with $V_0 = 0.4$. To trigger the KHI, we perturb the system at $t = 0$ by setting $V_y(x, y) = \epsilon V_0\ \sin(kx) exp(-y^2/\Delta)$ with the

perturbation amplitude $\epsilon = 0.05$ and KH wavenumber $k = 2\pi/\lambda = 2\pi/0.2$. The square simulation box size in the $x - y$ plane is $x = [0,\, L_x]$ and $y = [-L_y,\, L_y]$, with dimensionless $L_x = 2L_y = 1.5$. Therefore, the interface layer between two fluids is set at $y = 0$ line parallel to the x axis. The number of grid points is $N_x = N_y = 800$, so the spatial grid sizes are $\Delta x = \Delta y = 0.0018$. We have also two extra runs with larger grid points $N_x = N_y = 1500$. In addition, the CFL condition determines the time step at every integration cycle. Considering the assumption that $\Delta << L_y$, the density and velocity profiles are approximately step functions. This means that for $y < 0$ the velocity is $\mathbf{V}(y < 0) \approx -0.4\hat{\mathbf{x}}$ and $\rho(y < 0) \approx 1.0$, while for $y > 0$ the velocity is $\mathbf{V}(y > 0) \approx +0.4\hat{\mathbf{x}}$ and $\rho(y > 0) \approx 0.5$. Moreover, a uniform magnetic field parallel to the streaming flow is initially imposed in the form $\mathbf{B} = B_0\,\hat{\mathbf{x}}$ with $B_0 = 0.01,\, 0.1$. We applied periodic and open (outflow) boundary conditions on the boundaries in the x and y directions, respectively.

Similar to our boundary conditions on the x and y directions (parallel and perpendicular to the flow stream, respectively), [28] have also considered the same conditions to discuss the nonlinear evolution of Magnetic KHI in an ideal plasma. However, other type of boundary conditions such as open on the x-direction and open or highly conductive on the y-direction have been considered in some publications. Indeed, when the simulation box size in the y-direction is large enough or the KHI is in the linear or early nonlinear regime, the results are almost independent of the type of boundary condition on the y-direction.

Table 1: Values of resistivity and the Lundquist number

Resistivity (η)	Lundquist Number ($S = L_x V_A/\eta$)
1.0×10^{-7}	1.5×10^{5}
5.0×10^{-7}	3.0×10^{4}
1.0×10^{-6}	1.5×10^{4}
5.0×10^{-6}	3.0×10^{3}
1.0×10^{-5}	1.5×10^{3}
1.0×10^{-4}	1.5×10^{2}
5.0×10^{-4}	3.0×10^{1}
1.0×10^{-3}	1.5×10^{1}
5.0×10^{-3}	3.0×10^{0}

3 SIMULATION RESULTS and DISCUSSION

Considering the initial profiles, parameters, and simulation setup, we now run the 2D MHD PLUTO code to study the resistive KHI in a magnetized compressible plasma. The main focus is mostly on the magnetic energy features of KHI. Figure 1 plots the spatiotemporal variation of magnetic flux contours, ψ, defined by $\mathbf{B} = \nabla \times (\psi\hat{\mathbf{z}})$, in the $x - y$ plane for three values of plasma resistivity $\eta = 1.0 \times 10^{-5},\, 5.0 \times 10^{-4},\, 5.0 \times 10^{-3}$ with the same initial magnetic field $\mathbf{B}^{(0)} = B_0\hat{\mathbf{x}} = 0.01\hat{\mathbf{x}}$. In the absence of initial perpendicular components $V_z^{(0)}$ and $B_z^{(0)}$, the corresponding perturbed components $B_z^{(1)}$ and $V_z^{(1)}$ cannot be generated.

According to Figure 1, for all cases of η, magnetic field lines are gradually deformed from the initial parallel configuration by the KHI, and deformation increases as the KHI proceeds to the nonlinear regime. For comparison, for the case of minimum value, $\eta = 1.0 \times 10^{-5}$ magnetic field lines are highly distorted, Figure 1(j), compared with the case of maximum value $\eta = 5.0 \times 10^{-3}$, Figure 1(l). The extent of deformation can be equivalently monitored by calculating the electric current density which measures the amount of magnetic field

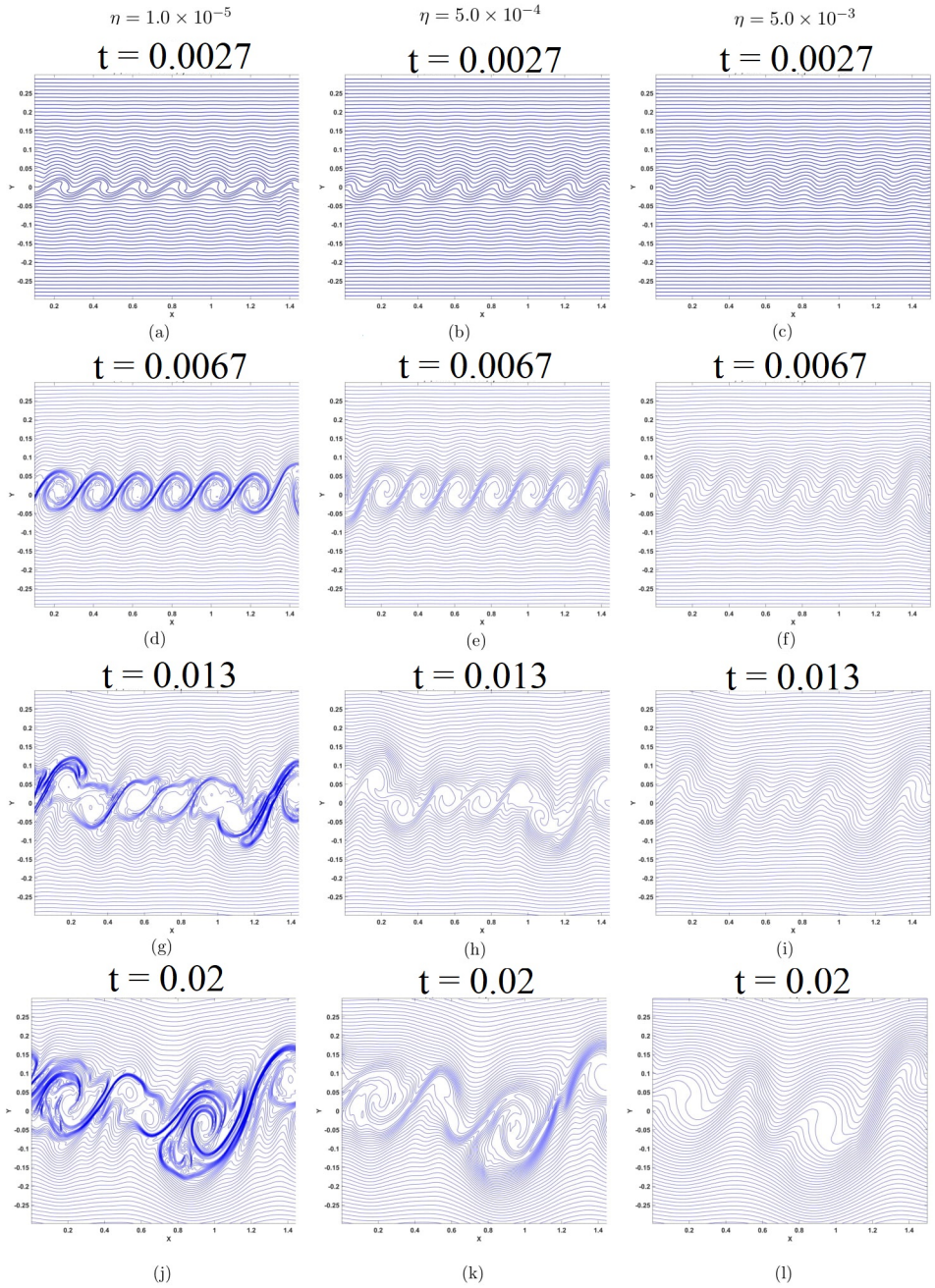

Figure 1: Contours of magnetic flux function, ψ, at different times for $\eta = 1.0 \times 10^{-5}$(left column); $\eta = 5.0 \times 10^{-4}$(middle column); $\eta = 5.0 \times 10^{-3}$(right column).

circulation at each point according to Ampere's law, $\mathbf{J} = \nabla \times \mathbf{B}$. Since, $\partial/\partial z = 0$, (i.e., 2D simulation), the only generated current density component is J_z, the perpendicular one. In Figure 2 we explore the absolute value of current density averaged over the simulation domain, $\tilde{J}_z = (\sum |J_z(x,y)|)/(N_x N_y)$, which indicates that $\tilde{J}_z$ increases with the evolution of KHI and its magnitude is larger for a lower resistivity, which verifies that the resistivity suppresses the evolution of magnetic file lines.

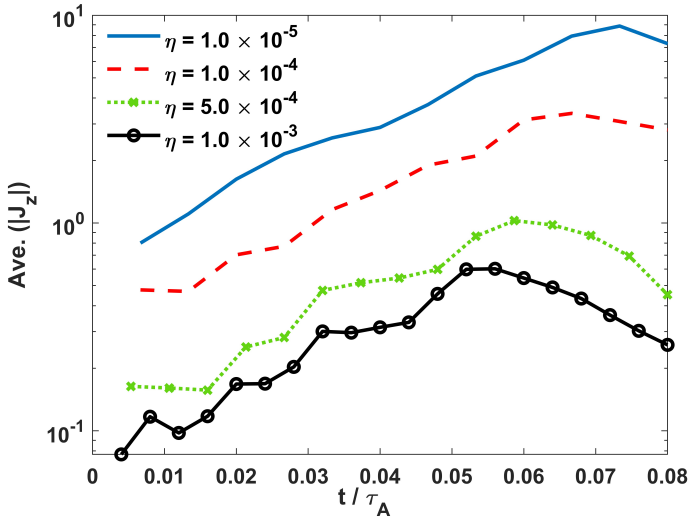

Figure 2: Time variation of the average of the absolute value of current density over simulation domain, $\tilde{J}_z$, for different values of resistivity.

Furthermore, magnetic field lines are strongly frozen on the plasma flow in the lower resistivity values, for which the plasma is relatively less collisional. Therefore, as the KHI develops from a linear regime into a fully nonlinear regime (turbulent), the topology of magnetic field lines mimics the pattern of plasma flow and KH vortices wrap up the field lines onto themselves. However, as the resistivity increases to a larger value, the plasma becomes more collisional, consequently, the motion of magnetic field lines decouples from the plasma flow due to the non-ideal effect of resistivity. This means that the magnetic field is now permitted to diffuse freely without any constraint imposed by plasma flow. Under this condition, there is an opportunity for a magnetic reconnection phenomenon to onset in some localized narrow regions inside the highly complex topology of magnetic field lines. Although the essential features of plasma density and velocity remain almost similar regardless of the change in resistivity (see the density continuity equation), the associated spatio-temporal evolution of the magnetic field is considerably affected by the increase of resistivity, which can be visually seen from Figure 1.

To examine the effect of finite uniform plasma resistivity on the temporal variation of magnetic field and its corresponding energy during the KHI, we show the time variation of total perturbed magnetic energy, $E^{(1)}_{mag} = E^{tot}_{mag} - E^{(0)}_{mag}$, for seven different values of plasma resistivity in Figure 3. Here, time and magnetic energy are normalized to the characteristic Alfvén time, $\tau_A = L_x/V_A = L_x\sqrt{\rho^{(0)}_{max}}/B_0$, and total energy of the system at $t = 0.$, $E_t(t=0)$, respectively, with $\rho^{(0)}_{max} = 1.0$ and $B_0 = 0.01$. According to Figure 3, for all cases of resistivity, three distinct phases can be observed; in the very early times of instability

which corresponds to the linear phase, the perturbed magnetic field is generated, and so the corresponding magnetic energy grows with time very fast, however, duration of the linear regime is very short. Then as the instability develops into the nonlinear phase, the growth rate naturally decreases remarkably but is still positive. Eventually, the magnetic energy increase saturates at a specific time, $t_s(\eta)$. Saturation results from a balance between magnetic energy production and dissipation mechanisms during the KHI. Note that, the decrease of magnetic energy at very late times of simulation is attributed to the outflow of magnetic energy from the up, $y = +L_y$, and down, $y = -L_y$, open boundaries following the formation of giant vortices with the sizes on the order of simulation box. Our attention is focused on the physics of KHI happening at relatively small time scales when the results are independent of the up and down boundary condition.

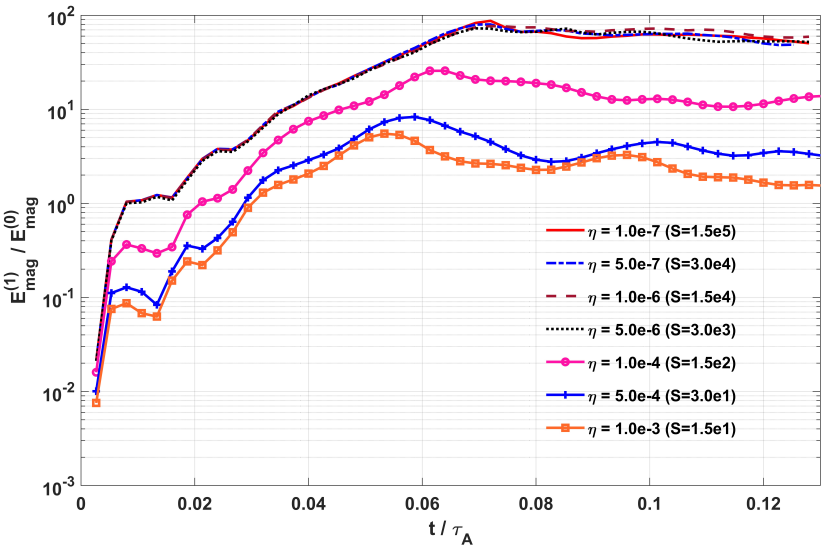

Figure 3: Temporal variation of the normalized perturbed magnetic energy for different values of the plasma resistivity (color online).

Here, three points can be visually inferred from Figure 3; First: the growth rate of magnetic energy, calculated from the slope of curves seems to be almost independent of the resistivity in either the linear or early nonlinear regimes. Second: The final saturated value of magnetic energy is higher in the case of smaller resistivity. So the maximum perturbed magnetic energy for $\eta = 1.0 \times 10^{-7}$ (minimum resistivity) is almost 40 times greater than that for the case $\eta = 1.0 \times 10^{-3}$. In addition, for the case of minimum resistivity, the perturbed magnetic energy increases even up to four orders of magnitude. In other words, as the plasma becomes more collisional, the process for generating magnetic field during the KHI becomes weaker. It can be concluded that, for a strongly collisional magnetized KH instability, the corresponding mechanism for generating magnetic field can be completely suppressed. Third: saturation happens early on as the resistivity increases. For example $t_s(\eta_{max})/t_s(\eta_{min}) \approx 1.5$. The final point to note here is that for smaller resistivities less than $\eta = 5.0 \times 10^{-6}$, the temporal behaviour of perturbed magnetic energy is similar. In particular, in the linear and early nonlinear regimes there is no seen any differences.

Figure 4 plots the saturated value of the perturbed magnetic energy versus the Lundquist number, S, for two values of the initial magnetic field. The perturbed magnetic field is

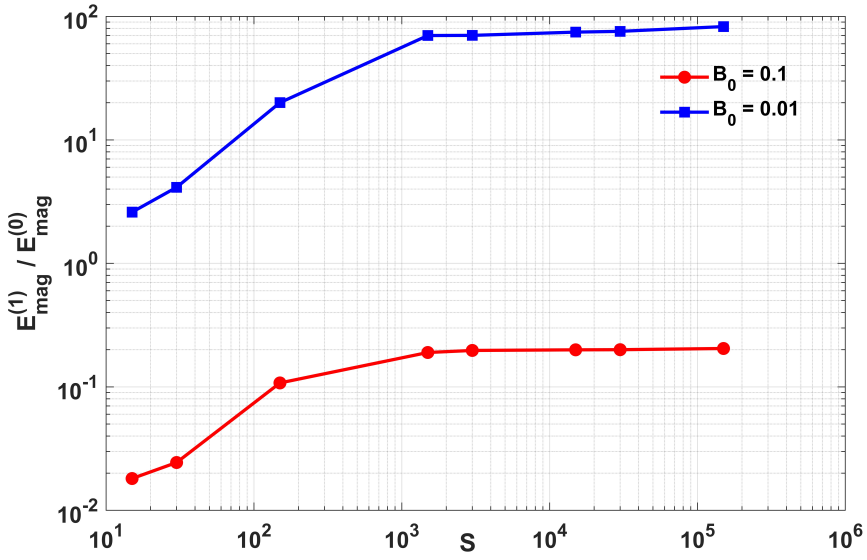

Figure 4: The normalized perturbed magnetic energy (R) versus the Lundquist number S for two values of the initial magnetic field.

normalized to the initial magnetic energy of the system. According to Figure 4, for both curves, as the Lundquist number, S, increases (resistivity decreases), the perturbed magnetic energy increases until it becomes saturated. However, the saturation value for $B_0 = 0.01$ is almost two orders of magnitude larger than the case of $B_0 = 0.1$. The linear dependency between the perturbed magnetic energy and the Lundquist number, S, at small values of S (or larger values of resistivity) can be inferred.

Now, let us investigate in more detail the generation mechanism of magnetic energy and its dependence on resistivity. To do so, for the case of $\eta = 5.0 \times 10^{-4}$, Figure 5 presents the temporal variation of the following four terms of the induction equation integrated over 2D spatial domain and time. Equation (2) is simply derived from the generalized Ohm's law inserted into Faraday's equation:

$$\underbrace{\int\int \Delta(\frac{\mathbf{B}^2}{2})dxdy}_{\text{term 1}} = \int_0^t \int_{-L_y}^{L_y} \int_0^{L_x} \left(\underbrace{-\nabla.[\mathbf{B} \times (\mathbf{V} \times \mathbf{B})]}_{\text{term 2}} \underbrace{-\mathbf{V}.\mathbf{J} \times \mathbf{B}}_{\text{term 3}} \underbrace{-\mathbf{B}.\nabla \times (\eta \mathbf{J})}_{\text{term 4}} \right) dxdydt. \quad (2)$$

We emphasize that all terms include integration over time and 2D space, and are normalized to the total magnetic energy at initial time, $E_{mag}(t = 0.)$ in the plot of Figure 5. We name the terms 1 to 4, as the "total perturbed magnetic energy", "convection", "flow's work on the magnetic field" and "resistive" terms, respectively. The "convection" term determines the amount of magnetic energy leaving the plasma volume by the convection motion of plasma (magnetic energy flux). The third term, $-\mathbf{V}.\mathbf{J} \times \mathbf{B}$ is the conversion rate of kinetic energy to magnetic energy via a work done by flow on the magnetic field.

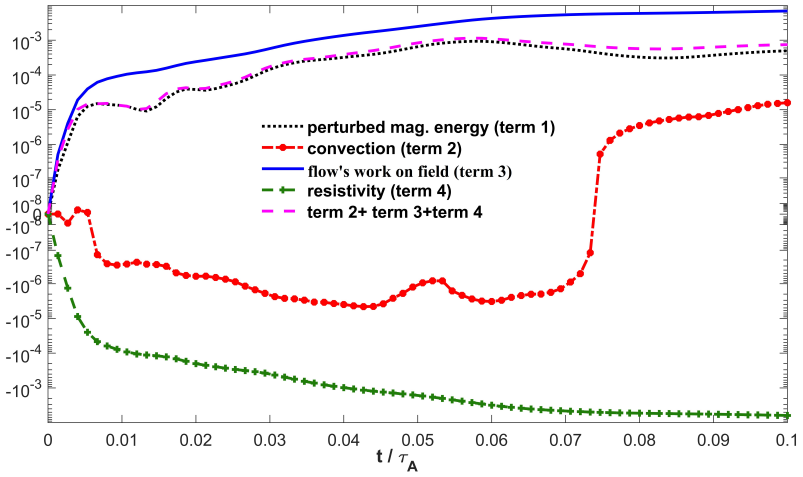

Figure 5: Temporal variation of different terms of the induction equation, Equation (1) (color online).

Terms 2 and 3, both represent the convection process, but as will be shown below in Figure 5, the contribution made by term 3 to the generation of magnetic energy is significant, therefore the appropriate name "flow's work on the magnetic field" is chosen. According to Figure 5, the "flow's work on the magnetic field" term (blue curve) is positive for the entire time duration of the simulation. From the very beginning of KHI, the flow works on the magnetic field and up to the short time $t/\tau_A \sim 0.005$, the corresponding term, term 3, increases linearly fast from zero to $\sim 10^{-4}$. Then, as the KHI transits into the nonlinear regime, the growth rate slows considerably until it becomes saturated at a magnitude $\sim 10^{-2}$. A comparison of this term with the temporal variation of perturbed magnetic energy (black curve) demonstrates that the work done by the flow on the magnetic field is the main mechanism for the generation of magnetic fields and magnetic energy. Opposite this, the "resistivity" term (green curve) is always negative, which means that it continuously dissipates part of magnetic energy via Joule (Ohmic) dissipation. As time goes on, the magnitude of resistive dissipation also increases. However, the amplification of magnetic energy by the work of flow always dominates the dissipation due to the resistivity effect. Both the amplification and the resistive dissipation become saturated at very late times of instability. This scenario of competition between amplification and dissipation agents, also explains the temporal variation of total perturbed magnetic energy already shown in Figure 3. Note that the magnitude of the "convection" term (term 2) highlighted in red color is almost three orders of magnitude smaller.

As the KHI develops, magnetic field lines are rolled up by flow vortexes, which leads to strong spatial gradients. So strong electric current densities are generated in elongated narrow layers, especially in regions where magnetic reconnection occurs. Thus, one expects an efficient process for generating the magnetic field as the KHI proceeds. Furthermore, for a larger resistivity value, the dissipation is basically stronger, leading to an earlier saturation of magnetic energy production by the work of flow. In our simulations when the resistivity increases from the minimum value of $\eta = 1.0 \times 10^{-7}$ to the maximum value 5.0×10^{-3}, the saturation of magnetic energy occurs at relatively earlier times (see Figure 3).

To find out more about the mechanism of magnetic field amplification, Figure 6(a,d,g)

plots the integrand of the term which represents the work done by plasma flow on the magnetic field, -$\mathbf{V}(x,y).(\mathbf{J}(x,y) \times \mathbf{B}(x,y))$, in three instants. The magnetic field generation is more efficient on the boundaries of growing KH vortices for a long time, where according to Figure 6(b,e,h) at these regions the current density, $J_z(x,y)$ is also significant. This matching can be seen clearly from Figure 6(c,f, i), in particular, in the early times of KHI, which presents the magnitude of J_z and $-\mathbf{V}.\mathbf{J} \times \mathbf{B}$ on the interface line ($y = L_y/2$). The similarity between the pattern of these terms indicates that the amplification is stronger at the locations where the electric current density is significant there. Therefore, on the boundaries of KH vortices, the magnitude of the perturbed magnetic field and its gradient are significant as expected.

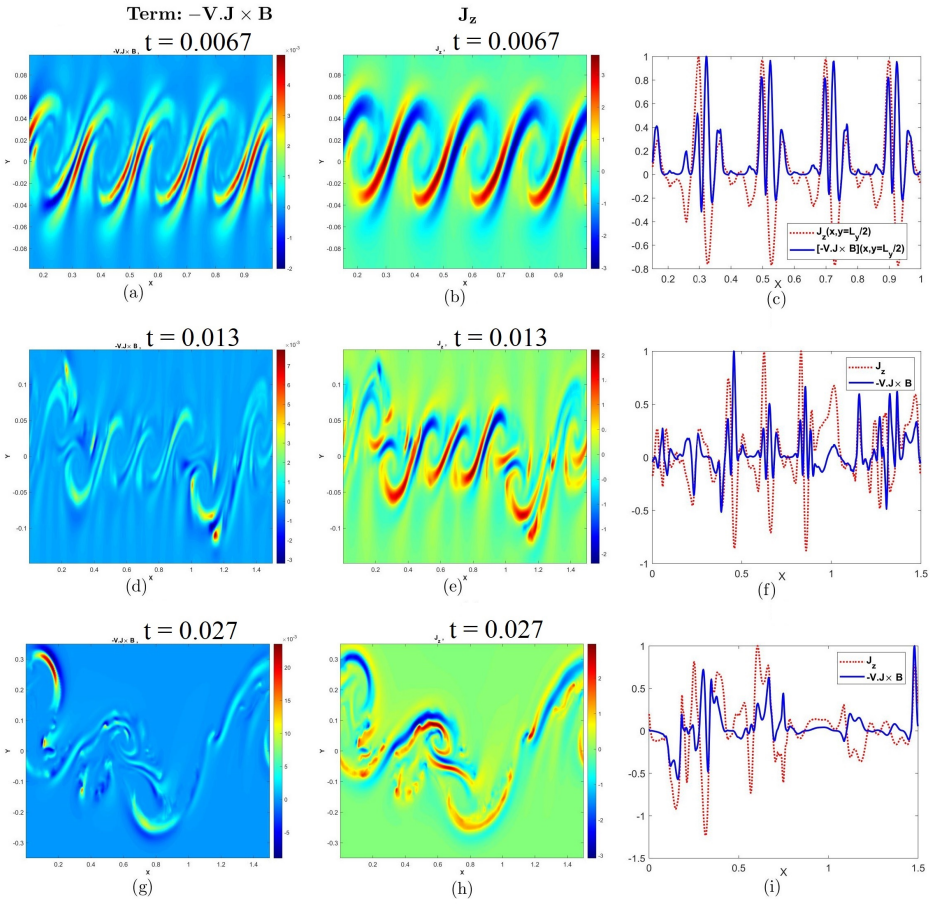

Figure 6: Variation of the term,$(-\mathbf{V}.\mathbf{J} \times \mathbf{B})$, and J_z in the $x-y$ plane (color online).

On the other hand, the main magnetic energy dissipation regions are those with significant localized current densities. Figure 7 depicts the spatial variation of dissipation rate ηJ_z^2 at three times. As seen, the boundaries of vortices are the main regions of magnetic energy dissipation. Interestingly, the generation of magnetic energy is also significant at these locations. In some of these regions, conditions for the magnetic reconnection phenomenon are satisfied, where magnetic energy is converted to other forms of energy such as kinetic energy of plasma. The X-points are the null points where magnetic reconnection

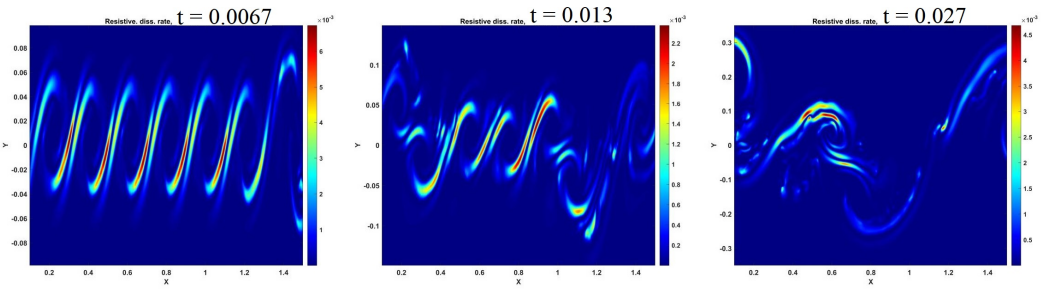

Figure 7: Variation of resistive dissipation rate, ηJ_z^2, in the $x-y$ plane for $\eta = 5.0 \times 10^{-4}$ at three times (color online).

occurs, and it is expected to observe many of them in the highly complicated configuration of magnetic field lines in the nonlinear regime of KHI. More X-points means more dissipation of magnetic energy via Joule heating. Within the highly turbulent structure of each giant vortice of KHI, one can detect some weak and highly transient reconnection events on very small scales which makes it difficult to count properly and accurately the number of formed X-points. The number of X-points, however varies with time and more importantly, the value of resistivity. To compare the dependency of X-point population on the plasma resistivity, we decided to count the X-points that appear clearly for a longer period on the spatial region where two monster vortices merge with opposite magnetic fields.

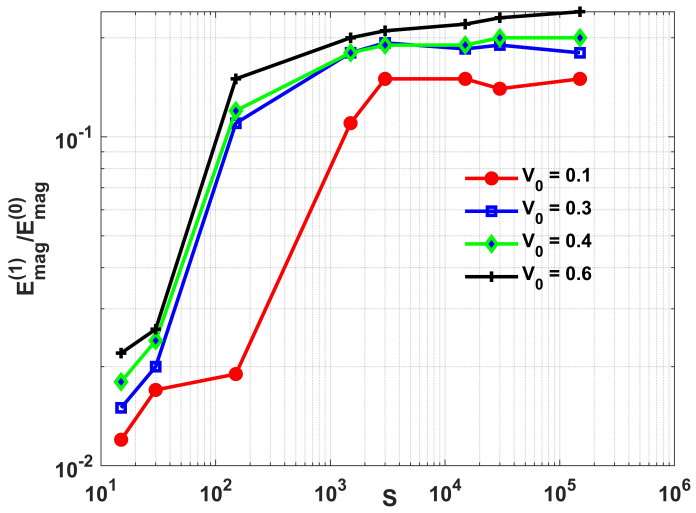

Figure 8: The normalized perturbed magnetic energy (R) versus the Lundquist number S for four values of the initial shear flow velocity V_0.

Our numerical simulation has three main parameters besides the plasma resistivity. First: The magnitude of initial shear flow velocity, V_0. Definitely, as the shear flow velocity decreases (increases), we expect a smaller (larger) growth rate of instability. We varied it to

be $V_0 = 0.1, 0.3, 0.4, 0.6$. Figure 8 plots the variation of the total perturbed magnetic energy normalized by the initial magnetic energy versus the Lundquist number (S) for different values of V_0. As expected, by increasing the magnitude of shear flow velocity, the instability grows faster and transits in a relatively shorter time scale from the linear to the nonlinear regime. Although, for all cases, we observe a saturation phase in larger values of the Lundquist number (smaller resistivity), however, for the case with a larger shear flow velocity, the magnitude of perturbed magnetic energy is relatively larger. One can conclude that regardless of the resistivity value (or the Lundquist number), the resistive Kelvin-Helmholtz instability with a larger initial shear flow velocity results in a stronger instability, and the amplification of the magnetic field is also stronger.

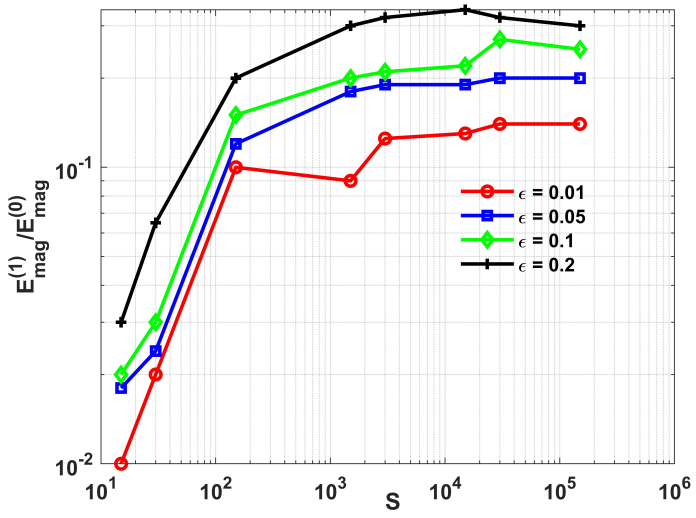

Figure 9: The normalized perturbed magnetic energy (R) versus the Lundquist number S for four values of the perturbation ϵ.

The second parameter is the amplitude of the initial perturbation (ϵ) perpendicular to the initial streaming. We examine four cases of $\epsilon = 0.01, 0.05, 0.1, 0.2$. Figure 9 plots the variation of the total perturbed magnetic energy normalized by the initial magnetic energy versus the Lundquist number (S) for different values of ϵ. As expected, by increasing the perturbation amplitude, the instability grows faster and transits in a relatively shorter time scale from the linear to the nonlinear regime. Although, for all cases, we observe a saturation phase in larger values of the Lundquist number (smaller resistivity), however, for the case with a larger perturbation amplitude, the magnitude of perturbed magnetic energy is relatively larger. We conclude that regardless of the resistivity value (or the Lundquist number), the resistive Kelvin-Helmholtz instability with a larger initial perturbation results in a stronger instability, and the amplification of the magnetic field is also stronger.

The last main parameter is the magnitude of the initial uniform magnetic field, B_0. We discuss the analysis for four cases of $B_0 = 0.001, 0.01, 0.1, 0.5$. Therefore, Figure 10 plots the variation of the total perturbed magnetic energy normalized by the initial magnetic energy versus the Lundquist number (S) for four different values of B_0. Larger values of the initial magnetic field, As described within the manuscript, larger values of the initial magnetic field, suppress the KHI and decrease the growth rate of instability. As a result, we expect

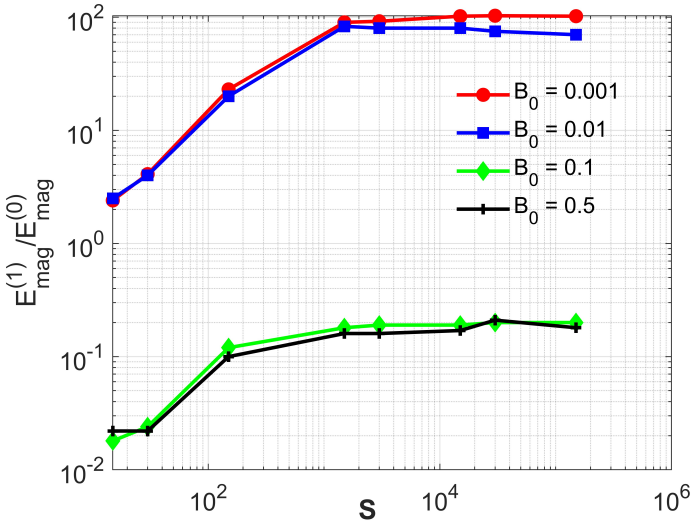

Figure 10: The normalized perturbed magnetic energy (R) versus the Lundquist number S for four values of the initial magnetic field B_0.

a weaker amplification of magnetic energy. This point can be seen clearly in Figure 10. However, the magnitudes of amplification for cases $B_0 = 0.001$ and 0.01 (smaller cases) are similar. Such a behavior is seen in larger cases of $B_0 = 0.1$ and 0.5.

4 SUMMARY AND CONCLUSION

Two-dimensional MHD numerical simulations are carried out to investigate the effect of finite uniform plasma resistivity on the Kelvin-Helmholtz instability in a magnetized compressible plasma. The main purpose was to study the spatio-temporal evolution of magnetic energy by varying plasma resistivity. To do so, we considered nine different values for plasma resistivity starting from $\eta = 1.0 \times 10^{-7}$ and increasing up to four orders of magnitude.

We found that as the KHI proceeds, the magnitude of perturbed magnetic energy increases with time until the saturation is achieved. The amplification of the magnetic field occurs very fast, in particular, in the linear regime. For example, for the case of $\eta = 1.0{\times}10^{-5}$ the perturbed magnetic energy is almost 30 times greater than the initial magnetic energy of the system, $R \equiv E^{(1)}_{mag}/E^{(0)}_{mag} \approx 30$ during saturation phase. This represents a powerful amplification with an efficient respective mechanism. It should be noted that such strong amplifications depend on the amplitudes of initial velocity parallel to the interface, V_0, and the y-component perturbation velocity, ϵV_0. Therefore weak ($V_0 << 1$) or strong ($V_0 \sim 1$) initial shear flows, weak ($\epsilon <\sim 0.001$) or strong ($\sim 0.1 < \epsilon <\sim 0.5$) perturbations would bring some changes at least to the numbers. In this study, we report the results with medium values of $V_0 = 0.4$ and $\epsilon = 0.05$. Nevertheless, observing numerically, such a considerable magnetic field amplification within short time scales with the medium values of parameters is promising.

Figure 4 plots the values of R versus S for two values of the magnetic field, $B_0 = 0.01$ and 0.1. For a smaller initial magnetic field, $B_0 = 0.01$, the amplification is also stronger than the case $B_0 = 0.1$. According to Figure 4, as the Lundquist number increases (resis-

tivity decreases), the value of R increases almost linearly in logarithmic axes for both cases $B_0 = 0.01$ and 0.1. In other words, for a less collisional KHI, the amplification of magnetic field, and so magnetic energy is considerably strong. Contrary to this, in a collisional plasma the amplification is relatively weak. Therefore, in some relevant space and astrophysical collisionless plasmas, one can expect strong magnetic energy amplification during the possible KHI. Understanding the main mechanisms of stable magnetic field production in astrophysical plasmas is still an open question. Since, the conditions for triggering KHI on a small or large scale can be easily satisfied in many space and astrophysical environments, our findings can be interesting. In essentially collisional laboratory plasmas, however, the amplification of magnetic field under the KHI is not considerable, and so it is not an important point of discussion. We note that the saturation of magnetic field amplification occurs relatively earlier for collisional plasmas.

Furthermore, we conclude that the work done by the plasma flow on the magnetic field is responsible for generating magnetic field during the KHI. Although, the flow's work on the field is in charge of magnetic energy production, on the other hand, plasma resistivity results in the dissipation of magnetic energy via Joule dissipation and its consequent conversion to other forms of energy. This dissipation essentially works in the regions where magnetic reconnection happens. In fact, following the fully nonlinear regime of KHI, the basic conditions for the magnetic reconnection process may appear temporarily in the compressed current sheets at the edges of the vortex rolls up and within the vortices. Both types I and II (discussed in the Introduction section) of magnetic reconnection during KHI are observed. We know that for a single magnetic reconnection process, the amount of magnetic energy released via the Joule heating increases naturally as the resistivity increases. However, during the magnetized KHI, as the resistivity increases, the results show that the growth of KHI decreases. As a result, the deformation of magnetic field lines from their initial straight-line configuration to complicated rolled-up field lines also decreases. This means that the system becomes less turbulent and the current sheets with opposite magnetic field lines where the reconnection occurs would appear rarely. Finally but interestingly, we observed the formation, merging, and eventually vanishing of a double current sheet, or a double tearing mode, for which the energy dissipation rate is relatively higher. The turbulent magnetic reconnection phenomenon during fully nonlinear KHI is still under investigation by researchers. However, in this study, we also investigated the general features of magnetic reconnection occurring in a specified current sheet. The temporal variation of the extent of asymmetry of magnetic field strength, the length-to-with ratio and reconnection rate are addressed.

In this study, we aimed to shed more light on the spatial and temporal evolution of magnetic energy and tried to discuss the main mechanism of magnetic energy amplification. Of course, there is still a need to consider the effect of varying some other parameters of KHI as mentioned. In our future study, we will investigate the amplification of magnetic energy on small scales and the role of magnetic reconnection in dissipating the energy by using particle-in-cell (PIC) simulations.

Acknowledgements

The author is very thankful to the Pluto code development team for making the code accessible for our simulations.

Authors' Contributions

The author contributed to data analysis, drafting, and revising of the paper and agreed to be responsible for all aspects of this work.

Data Availability

The raw data supporting the conclusions of this article will be made available by the authors, without undue reservation.

Conflicts of Interest

The author declares that there is no conflict of interest.

Ethical Considerations

The author has diligently addressed ethical concerns, such as informed consent, plagiarism, data fabrication, misconduct, falsification, double publication, redundancy, submission, and other related matters.

Funding

This research did not receive any grant from funding agencies in the public, commercial, or non profit sectors.

References

[1] Von Helmholtz, H. 1868, Monatsberichte der Königlichen Preussis-che Akademie des Wissenschaften zu Berlin, 23, 215.

[2] Kelvin, L. 1871, PMag., 42, 362.

[3] Chandrasekhar, S. 1961, Hydrodynamic and Hydromagnetic Stability, Oxford: Clarendon.

[4] Hasegawa, H., Sonnerup, B., Dunlop, M., Balogh, A., Haaland, S., & et al. 2004a, Ann. Geophys., 22, 1251.

[5] Hasegawa, H., Fujimoto, M., Phan, T.-D., Rème, H., Balogh, A., & et al. 2004b, Nature, 430, 755.

[6] Nykyri, K., Otto, A., Lavraud, B., Mouikis, C., Kistler, L. M., & et al. 2006, Ann. Geophys., 24, 2619.

[7] Nykyri, K. 2024, Geophy. Res. Lett., 51, e2024GL108605.

[8] Chaston, C. C., Wilber, M., Mozer F. S., Fujimoto, M., Goldstein, M. L., & et al. 2007, Phys. Rev. Lett., 99, 175004.

[9] Johnson, J. R., Wing, S., & Delamere, P. A. 2014, Space Sci. Rev., 184, 1.

[10] Kotsarenko, N., Lizunov, G., & Churyumov K. 1990, SvA Lett., 16, 113.

[11] Bucciantini, N., & Del Zanna, L. 2006, A&A, 454, 393.

[12] Boccardi, B., Krichbaum, T. P., Bach, U., Mertens, F., Ros, E., & et al. 2016, A&A, 585, A33.

[13] Walker, R. C., Hardee, P. E., Davies, F. B., Ly C., & Junor, W. 2018, ApJ, 855, 128.

[14] Chow, A., Davelaar, J., Rowan, M. E., & Sironi, L. 2023, ApJL, 951, L23.

[15] Ryutova, M., Berger T., Frank Z., Tarbell T., & Title A., 2010, Sol. Phys., 267, 75.

[16] Foullon, C., Verwichte, E., Nakariakov, V. M., Nykyri, K., & Farrugia, C. J. 2011, ApJL, 729, L8.

[17] Zhelyazkov, I., Zaqarashvili, T. V., & Chandra, R. 2015, A&A, 574, A55.

[18] Kieokaew, R., Lavraud, B., Yang Y., Matthaeus, W. H., Ruffolo, D., & et al. 2021, A&A, 656, A12.

[19] Ofman, L., & Thompson, B. J. 2011, ApJL, 734, L11.

[20] Zhelyazkov, I., & Chandra, R. 2020, Kelvin-Helmholtz Instability in Solar Atmospheric Jets, World Scientific Publication.

[21] Soler, R., Terradas, J., Oliver, R., Ballester, J. L., & Goossens, M. 2010, ApJ, 712, 875.

[22] Antolin, P., Yokoyama, T., & Van Doorsselaere, T. 2014, ApJ, 787, L22.

[23] Chhajlani, R.K., & Vyas, M. K. 1991, Astrophys. Space Sci., 176, 69.

[24] Min, K. W., & Lee, D. Y. 1996, Geophys. Res. Lett., 23, 3667.

[25] Howson, T. A., De Moortel, I., & Antolin, P. 2017, A&A, 602, A74.

[26] Palotti, M. L., Heitsch, F., Zweibel, E. G., Huang, Y.-M. 2008, ApJ, 678, 234.

[27] Mignone, A., Bodo, G., Massaglia, S., Matsakos, T., Tesileanu, O., & et al. 2007, ApJS, 170, 228.

[28] Malagoli, A., Bodo, G., & Rosner, R. 1996, ApJ, 456, 708.